Geophysical Research Letters

RESEARCH LETTER
10.1029/2022GL099892

Short-Lived and Voluminous Fluid-Flow in a Single Fracture Related to Seismic Events in the Middle Crust

D. Mindaleva[1], M. Uno[1], and N. Tsuchiya[1]

[1]Graduate School of Environmental Studies, Tohoku University, Sendai, Japan

Key Points:

- Fluid volumes estimated via reactive-transport modeling and thermodynamic analyses are used to approximate the moment magnitudes
- Moment magnitudes (−0.6 to 3.8) and short timescales of fluid infiltration (~10 hr) are comparable to slow-slip events
- Voluminous fluid flow in a single fracture may be related to the generation of crustal fracturing and the induction of short seismic events

Supporting Information:

Supporting Information may be found in the online version of this article.

Correspondence to:

D. Mindaleva and M. Uno,
diana@geo.kankyo.tohoku.ac.jp;
masa.uno@tohoku.ac.jp

Citation:

Mindaleva, D., Uno, M., & Tsuchiya, N. (2023). Short-lived and voluminous fluid-flow in a single fracture related to seismic events in the middle crust. *Geophysical Research Letters*, *50*, e2022GL099892. https://doi.org/10.1029/2022GL099892

Received 7 JUN 2022
Accepted 22 DEC 2022

Abstract This study focuses on samples that underwent rapid hydration (~10 hr) and evolved in permeability (~10^{-9} to 10^{-8} m^2) as a result of crustal fracturing. A coupled reactive transport model and thermodynamic analyses, focusing on Si alteration processes within reaction zones, are used to estimate the fluid volume required to induce fluid-driven seismic activity. Estimated fluid volumes (10^1–10^4 m^3) are used to approximate the moment magnitudes of potential seismic events. The resulting moment magnitudes (−0.6 to 3.8) and short timescales of fluid infiltration (~10 hr) are comparable to some slow-slip events, such as tremors and low-frequency earthquakes. This indicates that the voluminous fluid flow in a single fracture could be a key control on the generation of crustal fracturing and the induction of seismic activity above the tremor and slow slip events source regions in the lower–middle crust.

Plain Language Summary Short-lived fluid flow in the crust modifies the hydrological properties of rocks and controls the earthquakes triggering. However, there are limited numerical constraints on the fluid volumes that can be rapidly transported. This study focuses on fluid flow through a single fracture in metamorphic rocks. We discuss the relationship between estimated fluid volumes and a series of low-magnitude fracturing events, such as tremors and other types of slow slip events in the lower-middle crust. Specifically, we analyze unique geological and geochemical evidence preserved in fluid-rock reaction zones to approximate the duration of fluid infiltration and the volume of fluids transported. We use two independent methods for constraining generated seismic moment and magnitude based on fluid volumes and single fracture geometry. The transportation of fluid volumes through a fracture (10^1–10^4 m^3) may be related to short seismic events, as suggested by duration (~10 hr) and cumulative magnitude, representing the maximum values as 2.0–3.8. We observed a dramatic change in hydrological properties: from low permeable rocks to high-permeable fractures, which are not dead-end and can effectively transport a large volume of fluids in a short time. Such fluid infiltration can possibly trigger seismic activity above the earthquake source regions.

1. Introduction

Fluid flow in the crust induces hydration reactions and contributes to earthquake triggering (F. Cox, 1995; Kao et al., 2006; Oelkers & Helgeson, 1988; Sibson, 1994). Recent geophysical observations suggest that cyclic fluid infiltration is associated with slow-slip events (Obara, 2002; Ohmi & Obara, 2002; Shelly et al., 2006). These include episodic tremor and slip (ETS) events and low-frequency earthquakes (LFE), both of which occur within and outside of subduction zone (Ohmi & Obara, 2002; Rogers & Dragert, 2003) and are associated with surface displacement on the scale of millimeters, and can last for several hours (Bostock et al., 2015; Chestler & Creager, 2017; Nakamoto et al., 2021).

It is essential to analyze rock samples containing evidence of fluid activity to understand better the mechanisms of fluid infiltration and rock fracturing. Periodic seismic cycles are thought to comprise the accumulation of fluids derived from metamorphic dehydration reactions, a subsequent increase in fluid pressure, and fracturing (Audet et al., 2009; S. F. Cox, 2010; Peacock, 2009; Song et al., 2009). This fracturing enhances the permeability, providing additional fluid transport that may promote future seismic events (Audet & Bürgmann, 2014; Mukuhira et al., 2022; Nakajima & Uchida, 2018; Obara & Hirose, 2006; Ujiie et al., 2018; Warren-Smith et al., 2019). Determining the dynamic changes in fluid flux in the lower–middle crust is, therefore, key to advancing our understanding of the relationship between fluid infiltration and the triggering of seismic events.

It is difficult to quantify the amount of fluid transport within the crust, as this requires estimates of time-integrated fluid fluxes. This study constrains these fluxes using thermodynamic modeling of fluid chemistry, mass transfer, and hydraulic analysis to investigate the potential relationship between fluid behavior and local seismic events.

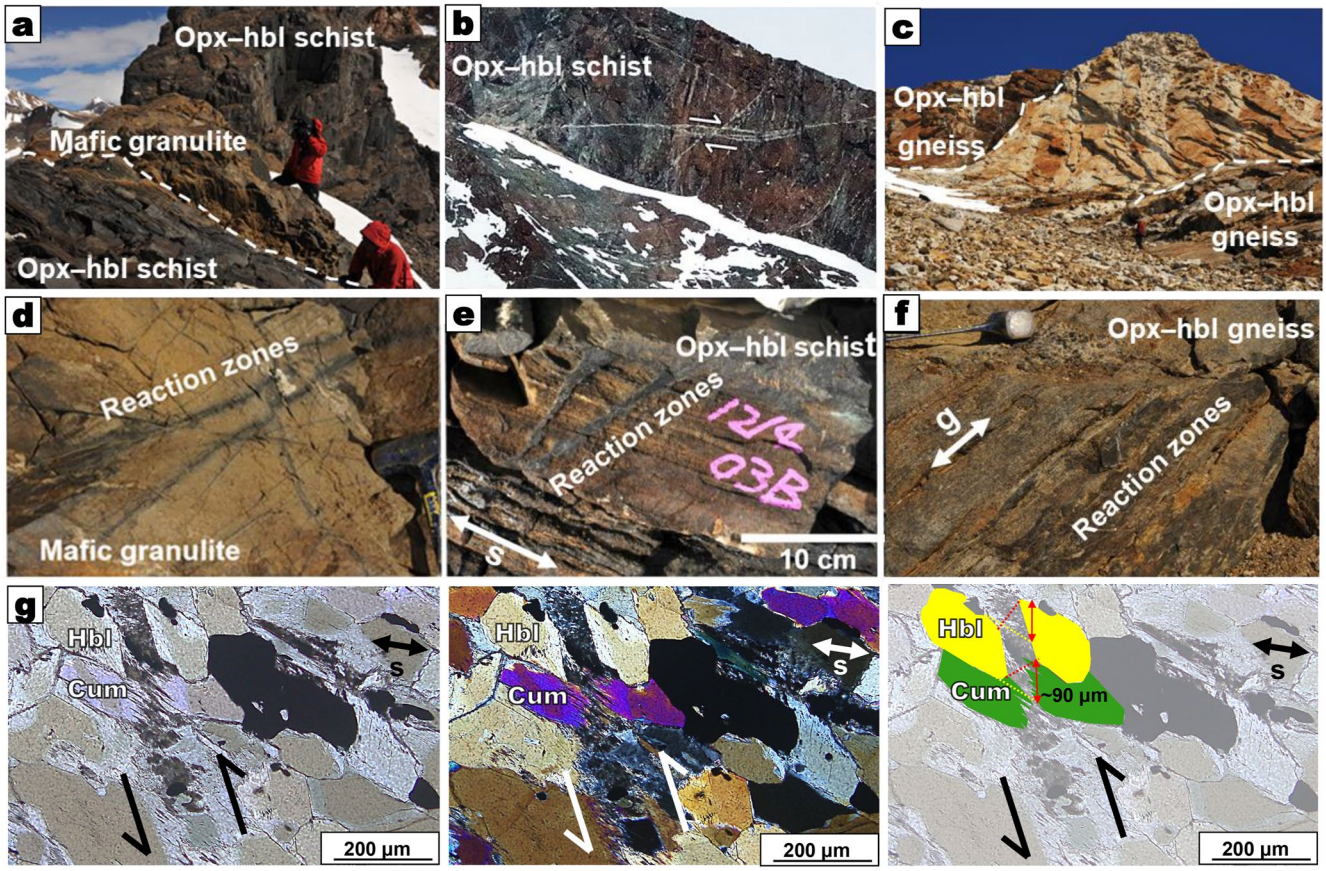

Figure 1. Photographs of representative examples and geological relationships in the study area. (a) Partly hydrated mafic granulite and orthopyroxene–hornblende (opx–hbl) schist; white dashed line indicates the boundary between mafic granulite and opx–hbl schist. (b) Partly hydrated opx–hbl schist and (c) opx–hbl gneiss. Reaction zones within (d) mafic granulite, (e) opx–hbl schist, and (f) opx–hbl gneiss. (g) Sinistral shear displacement along the fracture in the opx–hbl schist, yellow and green colors show the µm-scale offsets in the cummingtonite and hornblende grain boundaries. Note that orientation of hornblende and cummingtonite overgrowth within the fracture is controlled by the epitaxial growth from grains on the fracture wall, and not by the displacement. The section is perpendicular to the foliation and fracture. The "s" and "g" arrows indicate schistosity or gneissosity.

We used samples that provide information on the evolution of the permeability over short timescales of fluid infiltration, ranging from low-permeability wall rock to high-permeability reaction zones and fractures. The samples were mafic granulite and orthopyroxene–hornblende (opx–hbl) schist (Mindaleva et al., 2020) from the Mefjell area and opx–hbl gneiss samples from the Brattnipene area, both in the high-temperature metamorphic terrain of the Sør Rondane Mountains (SRM), East Antarctica (Figures 1a–1c).

Previous research in these areas has identified the activity of chlorine (Cl)-bearing fluid (Higashino et al., 2019; Kawakami et al., 2017; Uno et al., 2017).

The samples have been partly hydrated under upper-amphibolite–granulite facies conditions and contain fluid–rock reaction zones (Figures 1d–1f and Figure 2) that were analyzed to constrain the timescales of fluid infiltration.

We used a reactive transport model based on the diffusion–advection equation with local equilibrium (Baumgartner & Rumble, 1988; Bickle & McKenzie, 1987; John et al., 2012; Philpotts & Ague, 2009) with Cl profiles measured in individual apatite or amphibole crystals (Figure 2d). Flow timescales as short as a few–tens of hours (~1–71 hr) (Mindaleva et al., 2020) were estimated for all of the samples (Table S1 in Supporting Information S1). Single fracture permeability for the samples was determined using the Poiseuille law, yielding results of 10^{-9} to 10^{-8} m^2 (Table S1 in Supporting Information S1).

The implications of this modeling are discussed in terms of adequately estimating time-integrated fluid fluxes. The results show that the estimated duration of fluid infiltration in our samples is similar to the duration of some

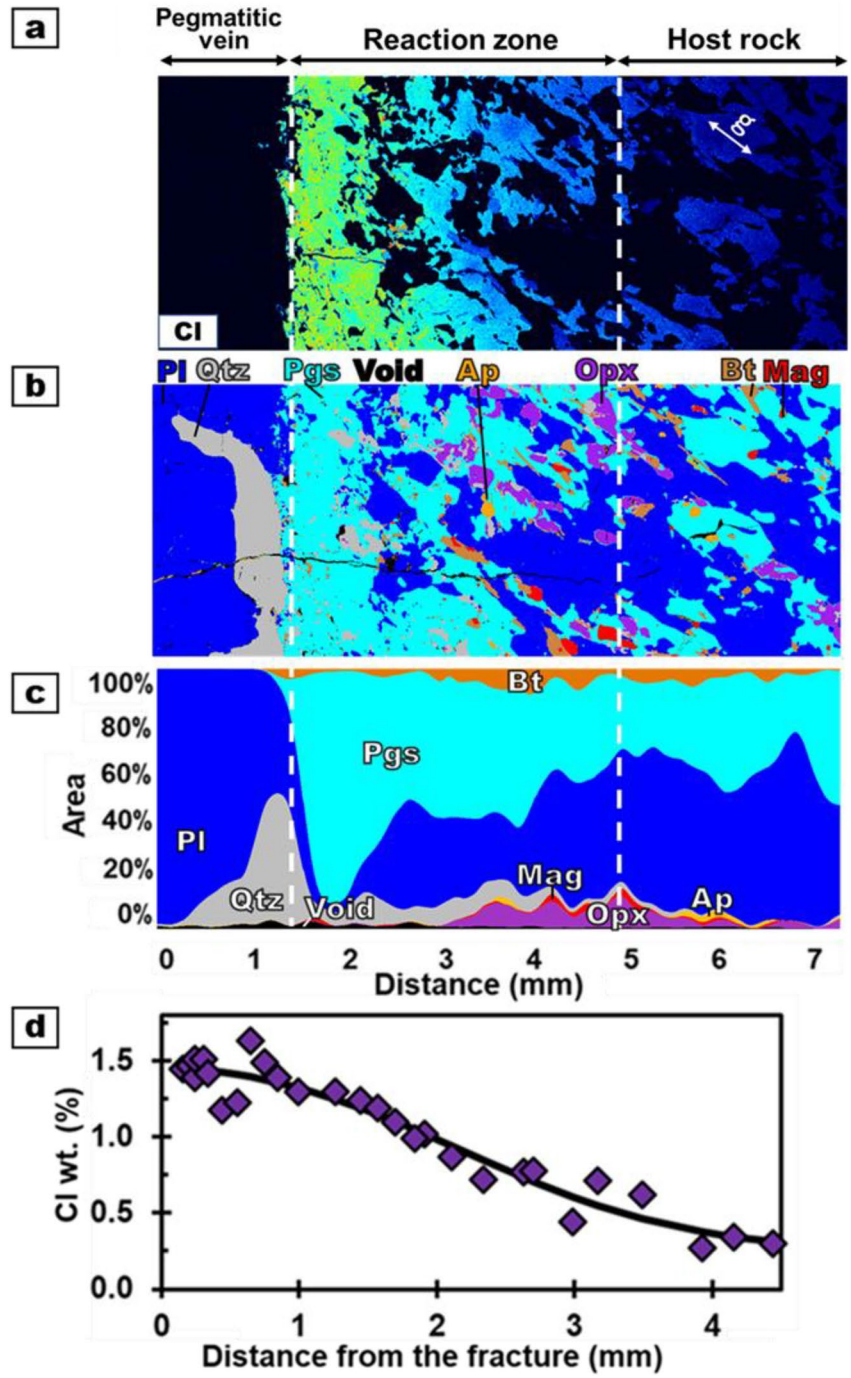

Figure 2. Distribution of chlorine concentrations in amphibole and modal mineralogy from the orthopyroxene–hornblende gneiss. The black line indicates the results of reactive transport modeling, and the arrow labeled "g" indicates the gneissosity. (a) Elemental map of chlorine; white dashed line indicates the boundary between pegmatitic vein, reaction zone, and host rock. (b) Mineral phase map made with XmapTools (Lanari et al., 2014). (c) Modal profile. (d) Chlorine profile measured in individual amphibole grains. The black lines are modeled fits by reactive transport modeling. Abbreviations: Qtz, quartz; Pl, plagioclase; Pgs, Pargasite; Bt, biotite; Opx, orthopyroxene; Mag, magnetite; Ap, apatite.

slow-slip events, such as tremors and LFEs. A methodology is proposed for estimating voluminous fluid fluxes through a single fracture, and the scaling of these results to a series of low-magnitude seismic events. This enables the coupling of petrology with the seismological implications of fracturing and fluid–rock interactions in the lower–middle crust.

2. Fracture-Related Hydrous Reaction Zones in Mafic Granulite, Orthopyroxene–Hornblende Schist, and Orthopyroxene–Hornblende Gneiss

The samples analyzed in this study located close to the Sør Rondane suture (Osanai et al., 1992, 2013; Shiraishi et al., 2008), a boundary between amphibolite- and granulite-facies rocks within the SW terrane of East Antarctica (Figure S1a in Supporting Information S1). Dark-colored hydrous reaction zones are present along fractures within the partially hydrated mafic granulite and opx–hbl schist samples (Figures 1d and 1e; Figure S1b and S1c in Supporting Information S1). The mafic granulite (Figure 1a) is weakly foliated and is cross-cut by reaction zones 5–30 m long and 0.2–2.0 cm wide (Figure 1d; Figure S1b in Supporting Information S1). The opx–hbl schist contains a well-developed schistosity. Reaction zones cross-cut the host rock oblique to the schistosity and are 5–30 m long and 0.3–3.0 cm wide (Figure 1e; Figure S1c in Supporting Information S1). An example of ∼0.1 mm sinistral offset of the grains on the wall of the shear fracture is shown in Figure 1g. The Brattnipene opx–hbl gneiss samples are either partly hydrated or contain pegmatitic veins (Figure 1f; Figure S1d in Supporting Information S1). These opx–hbl gneiss samples are cross-cut by reaction zones several millimeters to centimeters wide (Figure 1f; Figure S1d in Supporting Information S1) associated with 5–30 m long fractures. The 3 mm wide reaction zones occur between the veins and the host rock (Figure S1d in Supporting Information S1).

3. Mechanisms of Mineral–Fluid Reaction and Reactive Transport Modeling of Cl in Minerals

We observed Cl concentrations increasing in the apatites and amphiboles. We considered two possible mechanisms for mineral–fluids reaction: (a) a closed system with a desiccation process or (b) an open system with constant fluid flow and stable fluid composition.

Kusebauch, John, Whitehouse, and Engvik (2015), Kusebauch, John, Barnes, et al. (2015) provides Cl profiles in apatite with Rayleigh-distillation type fractionation. However, there are opposite trends compared to our samples; in their cases, Cl concentration gradually increases from the shear zone to the gabbro. The gradual consumption of OH from the dilute fluids leaded to Cl accumulation in the gabbro instead of shear zone. Contrary, Cl concentrations are higher in the fracture than in the host rock in our samples (Figure 2d). Therefore, we consider an open system with constant Cl-bearing fluid flow along the fractures. This is also supported by the fact that P-T conditions for the reaction zone formation are lower than for the host rock, and mass transport from reaction zones toward host rock is present.

For each sample, we estimated rock/fluid partition coefficients (K_v) using the apatite/fluid partition coefficient for Cl ($K_d = 2.3$) from Kusebauch, John, Whitehouse, Klemme and Putnis (2015), which was determined at crustal conditions (400°C–700°C and 0.2 GPa) in an experimental study. Details are provided in the Supporting information. Interface-coupled dissolution-reprecipitation is considered as a plausible mechanism that can explain the incorporation of Cl with the timescale estimated from the Cl profile across the reaction zones (∼tens of hours).

4. Time-Integrated Fluid Fluxes Through Fractures and Reaction Zones and Their Corresponding Potential Seismic Moment and Magnitude

We calculated the time-integrated fluid fluxes through both fractures and reaction zones (Figure S2a and S2b in Supporting Information S1, respectively) to understand the amount of fluid that could be transported through a single fracture within the lower–middle crust. Reaction zone time-integrated fluid fluxes were estimated from the flux required to account for the observed water content within the reaction zones (Q_{RZ}^{H2O}; $m^3\ m^{-2}$) and the flux required for chlorine transport toward the reaction zones (Q_{RZ}^{Cl}; $m^3\ m^{-2}$). Porosity data used to estimate Q_{RZ}^{Cl} are available through Ganzhorn et al. (2019), Saito et al. (2016), Vitovtova et al. (2014) and Katayama et al. (2012) and viscosity data are from Hack and Thompson (2011) and Huber et al. (2009),Fracture time-integrated fluid fluxes were estimated from the fluid flux required for silicon (Si) alteration in the reaction zones (Q_{FR}^{Si}; $m^3\ m^{-2}$) and the fluid flux estimated from the hydraulic permeability of the fracture, which is geometrically constrained using the fracture aperture (Q_{FR}^{Hyd}; $m^3\ m^{-2}$). Silicon solubilities are dependent on the pressure–temperature (P–T) gradients during metamorphism as a result of dissolution–precipitation processes. The modal mineralogy of the reaction zones undergoing decompression cooling is dependent on fluid Si solubilities. The Si solubilities for each sample were calculated using the bulk composition of each reaction zone for a range of P–T conditions and

were used to estimate fluid fluxes, given the relatively low sensitivity of these solubilities to variations in the Cl content of the fluid (Figure S3 in Supporting Information S1). Details of this analysis are provided in the Figure S3 in Supporting Information S1. The resulting estimates of reaction zone fluid fluxes ($\log_{10} Q_{RZ}^{H2O}$) are −4.2, –4.1, and –4.4 $m^3\ m^{-2}$ for the mafic granulite, hbl–opx schist, and hbl–opx gneiss samples, respectively (Table S1 in Supporting Information S1; Figure 3a).

The estimated fluxes required for Cl transport ($\log Q_{RZ}^{Cl}$) are −4.0 to −3.0 $m^3\ m^{-2}$, –4.1 to −3.1 $m^3\ m^{-2}$, and –4.4 to −3.4 $m^3\ m^{-2}$ for the mafic granulite, hbl–opx schist, and hbl–opx gneiss samples, respectively, and are of the same order of magnitude as the Q_{RZ}^{H2O} values (Figure 3a).

Fracture fluid fluxes derived from the total Si contents ($\log_{10} Q_{FR}^{Si}$) are 4.3–4.4, 5.8–6.1, and 4.5–4.8 $m^3\ m^{-2}$ for the mafic granulite, opx–hbl schist, and hbl–opx gneiss samples, respectively. Fluid volumes estimated from these Q_{FR}^{Si} values are 27–346 m^3, $1.2 \times 10^3\ m^3$ to $1.5 \times 10^4\ m^3$, and 35–438 m^3 for the mafic granulite, opx–hbl schist, and hbl–opx gneiss samples, respectively. Fluid fluxes estimated from fracture permeability, pressure gradient, assumed as lithostatic-hydrostatic difference (Table S1 in Supporting Information S1), and fluid infiltration timescales ($\log_{10} Q_{FR\delta}^{Hyd}$) are 3.8–5.6, 4.3–5.9, and 3.4–5.6 $m^3\ m^{-2}$ for the mafic granulite, hbl–opx schist, and hbl–opx gneiss, respectively (Table S1 in Supporting Information S1). For the opx–hbl schist sample, the fracture aperture estimated from X-ray elemental maps was 2.5 times wider than that for the other samples (Table S1 in Supporting Information S1; Figure 3a). The crack aperture during fluid infiltration is likely to have been wider as a result of fracture opening (Liu, 2005), as inferred from a comparison with $\log_{10} Q_{FR}^{Si}$. The calculated parameters are summarized in Table S1 in Supporting Information S1 and Figure 3a, which show that the two approaches yielded similar ranges. The fluid flux through the fracture was much higher than the fluid flux through the reaction zone, suggesting that more fluid was transported through the fracture with less fluid stored in reaction zones. This indicates that a much larger volume of fluid flows through the middle to lower crust, and therefore the analyzed fractures are transporting fractures and not dead-ended ones.

We used fluid fluxes to estimate the potential seismic response due to the fluid infiltration. The relationship between the fluid flux volume (ΔV) and cumulative seismic moment (ΣM_0) was proposed by McGarr (1976, 2014) as follows:

$$\Sigma M_0 = G\Delta V \tag{1}$$

where G is the shear modulus, which is assumed to be 4×10^{10} Pa for amphibolite facies rocks (Ji et al., 2013).

The important assumption is that the McGarr model predicts the maximum seismic moment for the saturated rocks in the region weakened by the pore pressure (McGarr, 2014). The actual seismic moment could be lower. For example, in permeable rocks, no stress accumulation occurs with fluid injection, and fracturing will not correspond to a seismic response. However, we observed the permeability evolution between the low permeable host rock ($\sim 10^{-22}\ m^2$) and fractures ($\sim 10^{-8}\ m^2$), so it is more likely that the accumulation of fluids leads to strain and stress efficiently. The following solid solution models were used to estimate host rock permeability: T. Holland and Powell (1996); Fuhrman and Lindsley (1988); Powell and Holland (1999); Wei and Powell (2003).

The seismic moment for a single fracture derived from the fracture geometry was also estimated based on the definition of the seismic moment:

$$M_0 = \mathrm{GAD} \tag{2}$$

where A is the cross-section of the fracture (m^2) and D is the average slip on A (m). Based on the occurrence of the fractures, we used 5–30 × 5–30 m cross sections for all of the samples and $D = 0.1$ mm.

The moment magnitude (M_w) is derived from the seismic moment as follows (Kanamori, 1977; Kanamori & Brodsky, 2004):

$$M_w = 2/3 \log_{10}(M_0) - 6.07 \tag{3}$$

The estimated results of the cumulative seismic moment and seismic moment for a single fracture derived from the fracture geometry and fluid volume are shown in Figure 3b.

Estimates of the cumulative seismic moment based on fluid volume are 1.1×10^{12} to 6.1×10^{14} Nm for all samples. Estimates of the seismic moment for a single fracture based on fracture geometry are 1.7×10^8 to

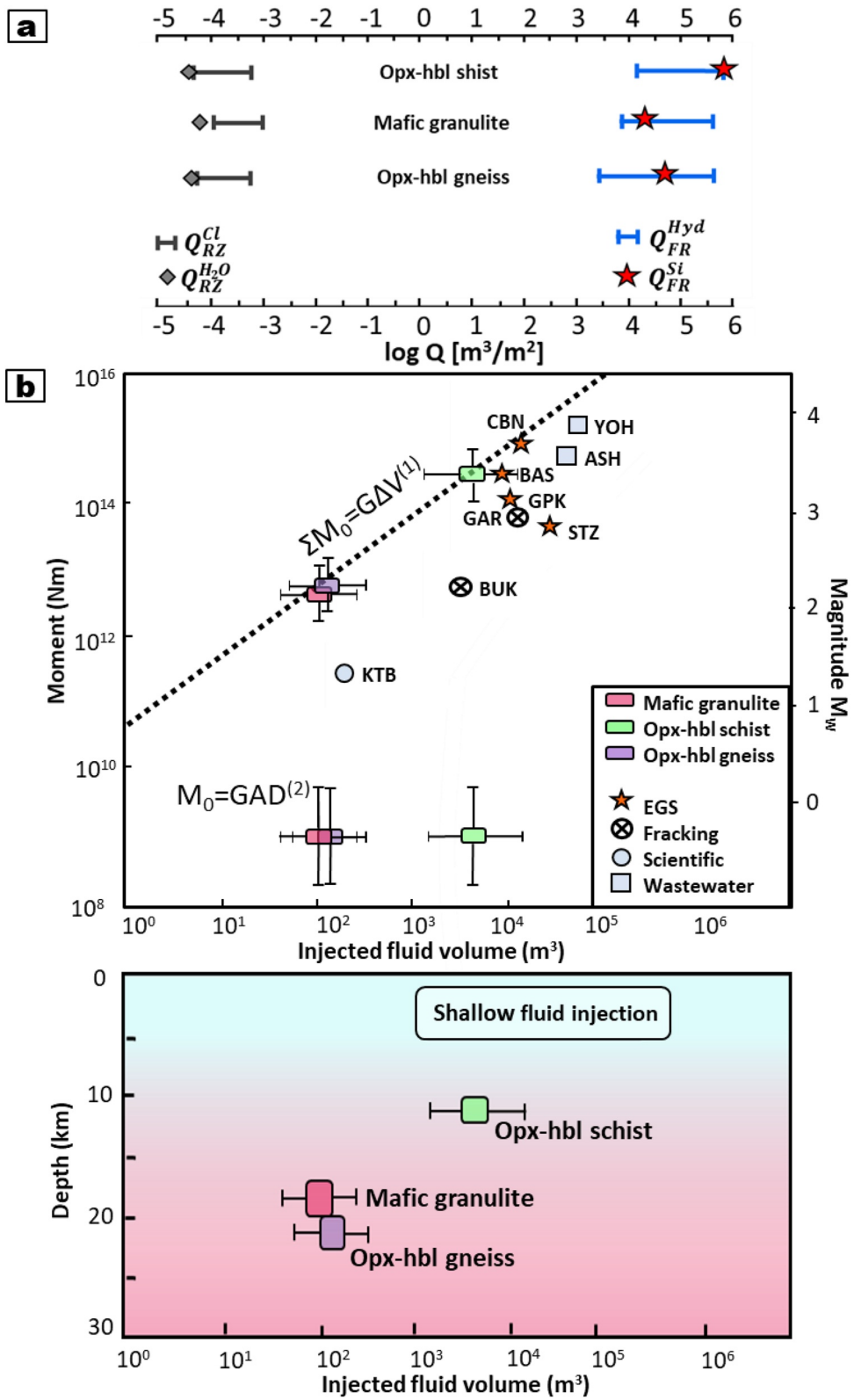

Figure 3.

2.1×10^9 Nm. Different moment magnitudes are therefore estimated from these seismic moments, yielding moment magnitudes of 2.0–3.8 for the cumulative seismic moment and −0.6 to 0.2 for the seismic moment for a single fracture, as derived from fracture geometry (Table S1 in Supporting Information S1; Figure 3b). It is noted that geophysical observations may not detect the signal generated by sub mm-scale displacement in the lower–middle crust. The observation of μm-scale displacement (90 μm) along the fracture in the shear wall (Figure 1g) provides evidence of shear fractures in the lower-middle crust and their potential relation to seismic events as below.

5. Discussion

Timescale is an important parameter for time-integrated fluid flux estimations. Short timescales of fluid infiltration (1–71 hr) estimated in this study are not common compared to previous studies (i.e., months to thousands of years; John et al., 2012; Kleine et al., 2016; Taetz et al., 2018). Flux through the vein from Beinlich et al. (2010) provides $10^{5\pm1}$ m^3/m^{-2}. The flux through the vein in our samples with ∼30 μm in aperture width provides similar values. A comparison of the estimated fluid fluxes through the fracture (10^{3-6} m^3/m^2) to the Zack and John (2007) and Ague (2003) (Figure S4 in Supporting Information S1) shows that lower ranges are similar to the fluxes through the upper crustal fracture zones (10^{3-4} m^3/m^{-2}), while upper ranges are comparable to the flux through the quartz veins ($\sim10^{3-5}$ m^3/m^{-2}). Compared to previous works, time-integrated fluid fluxes through the fracture estimated in this study show that large fluxes could be achieved in shorter timescales.

The transport of high volumes of fluid (10^1–10^4 m^3) through the fractured crust is essential to explain the role of fluids in triggering seismic events (Figure 3b).

Fluid injection experiments are depth-limited, and geophysical observations cannot provide information on the fluid volumes. The results obtained from the high-grade schists and gneisses were combined with fluid injection data (Baisch et al., 2006, 2010; Bickle & McKenzie, 1987; Dorbath et al., 2009; Evans et al., 2005; Horálek et al., 2010; Mukuhira et al., 2008) to determine the behavior of fluids during fracturing events that are likely related to ETS and LFE (Figure 4). The rocks expected along subduction boundaries where most of the short-term slow slip events (SSEs) detected are relatively low temperature compared to this study. However there are some examples detected in a continental plate boundary faults, including the continental collision zone in Taiwan at depths of 15–45 km (Chen et al., 2018), the strike-slip San Andreas Fault in California (Shelly, 2017), and the oblique right-lateral Alpine Fault in New Zealand (Wech et al., 2012).

High fluid fluxes (10^1–10^4 m^3) induce rock fracturing, enhancing the permeability ($\sim10^{-9}$ to 10^{-8} m^2) of potentially seismogenic regions. These fractures close during the periods between slip episodes, forming hydrous mineral reaction zones that decrease permeability $\sim10^{-22}$ to 10^{-20} m^2 (Mindaleva et al., 2020). Therefore, episodic fluid flux is likely to control the permeability evolution and the voluminous fluid transport within the crust.

Fluid injection experiments in upper crustal rocks have determined the relationship between the volume of fluid and swarm seismicity. The injection of large fluid volumes into low-permeability rock induces seismicity that lasts from days to months. We compared fluid injection data with cumulative seismic moments derived from fluid volumes and the seismic moments obtained from the geometry of the single fractures (Figures 3b), (Supporting Information S1).

The fluid volumes estimated for opx–hbl schist samples are similar to the shallow fluid injection results (Figure 3b), in contrast to the deeper mafic granulite and opx–hbl gneiss samples.

The cumulative moment and magnitude values outlined above are higher than single fracture-based seismic moment estimates (Table S1 in Supporting Information S1; Figure 3b). This suggests that a large amount of fluid can be transported through a single fracture in the lower–middle crust, although the magnitude of the resulting earthquake will be lower than the cumulative magnitude.

Figure 3. (a) Variations in fluxes through reaction zones (Q_{RZ}^{H2O} and Q_{RZ}^{Cl}; gray diamonds and solid lines, respectively) and a fracture (Q_{FR}^{Hyd} and Q_{FR}^{Si}; solid blue lines and red stars, respectively) within opx–hbl schist, mafic granulite, and opx–hbl gneiss samples. (b) Relationships between injected fluid volume (ΔV), cumulative seismic moment release (ΣM_0), and moment magnitude (M_w). The theoretical relationship between ΣM_0 and ΔV is from McGarr (1976). Cumulative seismic moment release $\Sigma M_0 = G\Delta V$ is compared to the seismic moment for a single fracture, based on fracture geometry M_0 = GAD. EGS indicates an enhanced geothermal system, and "wastewater" indicates wastewater injected to enhance permeability. Modified after McGarr (2014) and S. F. Cox (2016). Our Q_{FR}^{Si}-derived results are compared to fluid injection data predominantly for the upper crust. The KTB experiment (Brudy et al., 1997) was performed at ∼9 km depth, the deepest of the fluid-injection experimental data shown in this figure.

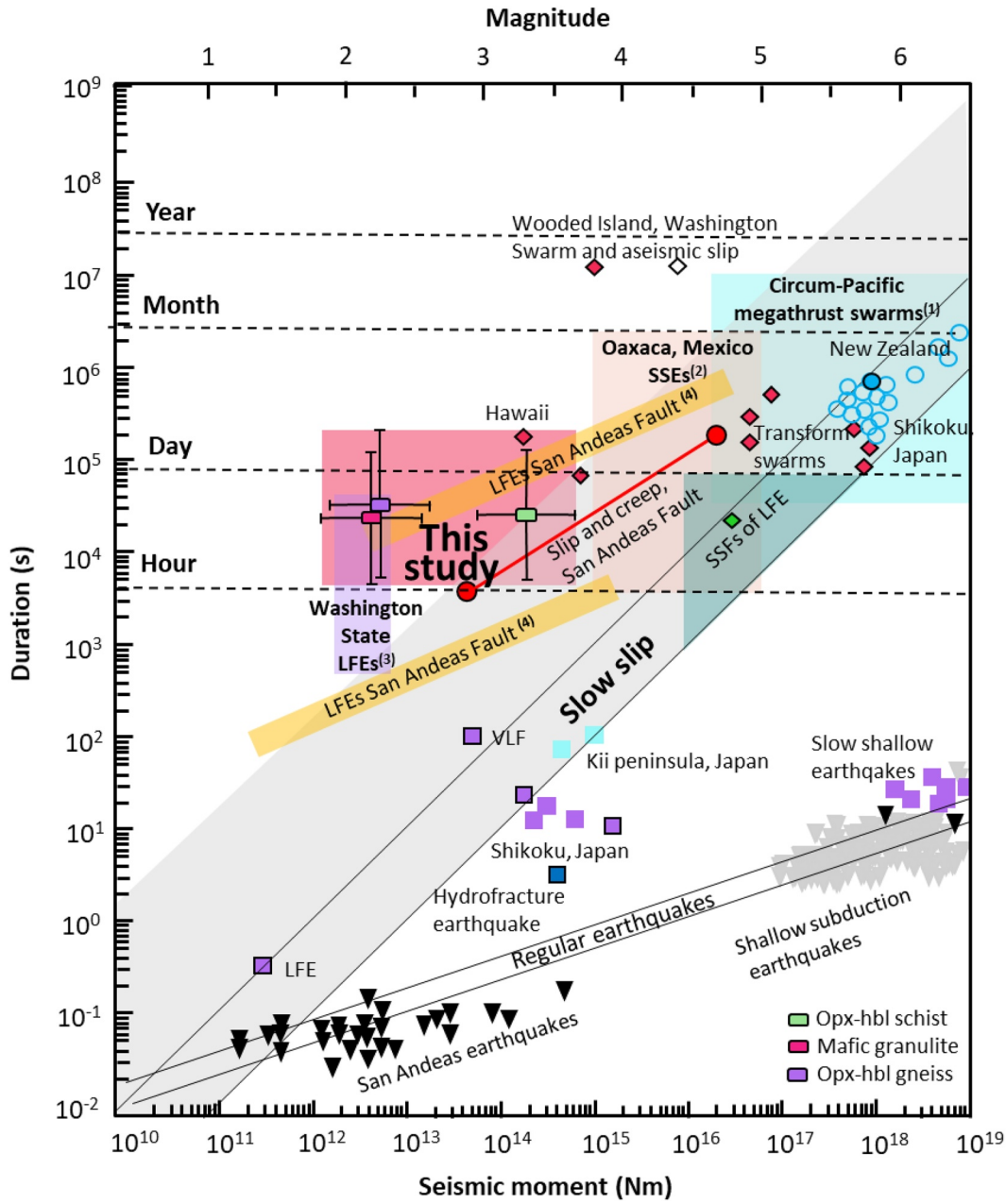

Figure 4. Event durations for swarms and individual earthquakes compared to the seismic moment and magnitude data. The gray shaded area between the black lines represents the moment–duration scaling law for slow slip phenomena from Ide et al. (2007) and Michel et al. (2019). The characteristics of fracturing events in the samples analyzed during this study are shown as red rectangle; the durations correspond to the duration of fluid activity. Data in this figure are from the following sources: (1) total seismic moment for Circum-Pacific megathrust swarms (light blue): Holtkamp and Brudzinski (2011); (2) total seismic moment release for short-term slow slip events in the Oaxaca region, Mexico (pink): Fasola et al. (2019); (3) cumulative swarm seismic moment for low-frequency earthquakes (LFEs), Washington State, USA (purple): Sweet et al. (2014); and (4) individual moment magnitude data for LFEs along the San Andreas Fault (orange): Tan and Marsan, (2020). Individual geodetic (open symbols) and seismic (filled symbols) measurements are from Ide et al. (2007) and Peng and Gomberg (2010).

Figure 4 compares the total duration and seismic moment and magnitude values of earthquake swarms, single events, SSEs, ETS events, LFEs, and very low-frequency earthquakes (VLFEs), (Supporting Information S1). These data allow the duration and individual/cumulative characteristics of fluid activity to be compared with the seismic/aseismic events (Figure 4).

Fluid activity may induce seismicity along fractures, with the cumulative magnitudes representing the maximum values (2.0–3.8) determined for the study area. In addition, the magnitude of a single fluid-driven fracturing event (−0.6 to 0.2) may represent the lower limit for a single seismic event. Fluid activity within reaction zones may be related to short seismic/aseismic events such as tremors and LFEs, as suggested by duration and magnitude estimates presented in this study (Figure 4). This study also provided the first estimates of the volume of fluid that could pass through a single fracture within the middle to lower crust, but in fact, the crust contains networks of such fractures. The relationship between seismic moment and duration in Figure 4 is based on a single fracture, meaning that the presence of fracture networks may cause the seismic moment and duration to increase.

6. Conclusions

This study presents the results of two approaches used to calculate fluid fluxes through a fracture: one that uses permeability, pressure gradient, and fluid infiltration timescales; and another that applies advective reaction–transport equations to the results of fluid speciation phase equilibrium modeling. Single fracture fluid fluxes are estimated to be several orders higher than fluid fluxes associated with reaction zones. The single fracture fluid fluxes ($\log_{10} Q$) are 3.8–5.6, 4.3–5.9, and 3.4–5.6 $m^3\ m^{-2}$ for mafic granulite, opx–hbl schist, and opx–hbl gneiss samples, respectively, whereas reaction zone fluid fluxes ($\log_1 0Q$) are −4.4 and –3.0 $m^3\ m^{-2}$ for all samples. These results demonstrate that fractures are effective pathways for transporting large amounts of fluid in the crust.

The short timescales and dynamic evolution of fluid flow through samples suggest that fluid infiltration may be related to seismicity. This type of process, whereby large volumes of fluid are transported over short timescales (i.e., 10^1–10^4 m^3 per a few hours), may be common above earthquake source regions. Fracture geometry-based seismic moment estimates vary from 1.7×10^8 to 2.1×10^9 Nm for all samples, yielding magnitudes from −0.6 to 0.2. Fluid volume estimates yield cumulative seismic moment values of 1.1×10^{12} to 6.1×10^{14} Nm with moment magnitudes of 2.0–3.8 for all samples. These data indicate the relationship between the volume of fluid transported within a single fracture and the seismic response to fracturing. This shows that the infiltration of large volumes of fluid through single fractures may be common during some slow-slip phenomena, including tremors and LFEs, as suggested by similarities in event duration and magnitude estimates. The earthquake magnitude of a single fluid-driven fracturing event in the lower–middle crust is potentially lower than that of a series of fracturing events. The present results also indicate that geological samples can provide unique information about single fluid-driven fracturing events recorded by metamorphic reaction zones. This study represents the first attempt to combine thermodynamic modeling estimations from reaction zone samples with clear numerically estimated timescales and permeabilities, thereby advancing our understanding of fluid infiltration in the lower–middle crust.

Acknowledgments
Authors Mindaleva, Uno, and Tsuchiya contributed equally to this work. Noriyoshi Tsuchiya contributed to fieldwork and the overall concept of the research and provided supervision. He has equivalent contributions to the research, but due to system limitations, we state that he is an equal corresponding author here; his email: noriyoshi.tsuchiya.e6@tohoku.ac.jp. We thank all members of JARE-51 for their assistance. T. Kawakami, M. Ishikawa, M. Satish-Kumar, G. Grantham. A. Okamoto, and R. Oyanagi are thanked for their critical comments and suggestions, and M. Toriumi is thanked for continued support and constructive discussions. We thank GRL editor Germán Prieto, reviewers Timm John and Simon Wallis for constructive improvements and valuable feedback. This study was supported in part by JSPS KAKENHI Grant K21K203740 awarded to DM; and JP15K17783, JP17H05310, JP18K13628, JP22H01329, JP22H05296, and JP22K18994, all awarded to MU. We acknowledge JP21H05200 and JP16K21728 for the support.

Data Availability Statement

The authors confirm that the data supporting the findings of this study are available within the article [and/or] its supporting information. Thermodynamic data used in the study is available through T. J. B. Holland and Powell (1998), (https://doi.org/10.1111/j.1525-1314.1998.00140.x). DEW aqueous database in Perple_X 6.8.7 (J. A. D. Connolly, 2009, https://doi.org/10.1029/2009GC002540) is available through Galvez et al. (2015) and Connolly and Galvez (2018), (http://dx.doi.org/10.1016/j.epsl.2015.06.019; https://doi.org/10.1016/j.epsl.2018.08.024).

References

Ague, J. J. (2003). Fluid flow in the deep crust. Treatise on geochemistry.

Audet, P., Bostock, M. G., Christensen, N. I., & Peacock, S. M. (2009). Seismic evidence for overpressured subducted oceanic crust and megathrust fault sealing. *Nature*, *457*(7225), 76–78. https://doi.org/10.1038/nature07650

Audet, P., & Bürgmann, R. (2014). Possible control of subduction zone slow-earthquake periodicity by silica enrichment. *Nature*, *510*(7505), 389–392. https://doi.org/10.1038/nature13391

Baisch, S., Vörös, R., Rothert, E., Stang, H., Jung, R., & Schellschmidt, R. (2010). A numerical model for fluid injection induced seismicity at Soultz-sous-Forêts. *International Journal of Rock Mechanics and Mining Sciences*, *47*(3), 405–413. https://doi.org/10.1016/j.ijrmms.2009.10.001

Baisch, S., Weidler, R., Vörös, R., Wyborn, D., & de Graaf, L. (2006). Induced seismicity during the stimulation of a geothermal HFR reservoir in the Cooper Basin, Australia. *Bulletin of the Seismological Society of America*, *96*(6), 2242–2256. https://doi.org/10.1785/0120050255

Baumgartner, L. P., & Rumble, D. (1988). Transport of stable isotopes: I: Development of a kinetic continuum theory for stable isotope transport. *Contributions to Mineralogy and Petrology*, *98*(4), 417–430. https://doi.org/10.1007/BF00372362

Beinlich, A., Klemd, R., John, T., & Gao, J. (2010). Trace-element mobilization during Ca-metasomatism along a major fluid conduit: Eclogitization of blueschist as a consequence of fluid-rock interaction. *Geochimica et Cosmochimica Acta*, *74*(6), 1892–1922. https://doi.org/10.1016/j.gca.2009.12.011

Bickle, M. J., & McKenzie, D. (1987). The transport of heat and matter by fluids during metamorphism. *Contributions to Mineralogy and Petrology*, *95*(3), 384–392. https://doi.org/10.1007/BF00371852

Bostock, M. G., Thomas, A. M., Savard, G., Chuang, L., & Rubin, A. M. (2015). Magnitudes and moment-duration scaling of low-frequency earthquakes beneath southern Vancouver Island. *Journal of Geophysical Research: Solid Earth*, *120*(9), 6329–6350. https://doi.org/10.1002/2015JB012195

Brudy, M., Zoback, M. D., Fuchs, K., Rummel, F., & Baumg'art, J. (1997). Estimation of the complete stress tensor to 8 km depth in the KTB scientific drill holes' Implications for crustal strength. *Journal of Geophysical Research*, *102*, 18453–18475.

Chen, K. H., Tai, H., Ide, S., Byrne, T. B., & Johnson, C. W. (2018). Tidal modulation and tectonic implications of tremors in Taiwan. *Journal of Geophysical Research: Solid Earth*, *123*(7), 5945–5964. https://doi.org/10.1029/2018JB015663

Chestler, S. R., & Creager, K. C. (2017). A model for low-frequency earthquake slip. *Geochemistry, Geophysics, Geosystems*, *18*(12), 4690–4708. https://doi.org/10.1002/2017GC007253

Connolly, J. A. D. (2009). The geodynamic equation of state: What and how. *Geochemistry, Geophysics, Geosystems*, *10*(10), Q10014. https://doi.org/10.1029/2009GC002540

Connolly, J. A. D., & Galvez, M. E. (2018). Electrolytic fluid speciation by Gibbs energy minimization and implications for subduction zone mass transfer. *Earth and Planetary Science Letters*, *501*, 90–102. https://doi.org/10.1016/j.epsl.2018.08.024

Cox, F. (1995). Faulting processes at high fluid pressures: An example of fault valve behavior from the Wattle Gully Fault, Victoria, Australia. *Journal of Geophysical Research*, *100*(289), 23–32. https://doi.org/10.1029/95jb00915

Cox, S. F. (2010). The application of failure mode diagrams for exploring the roles of fluid pressure and stress states in controlling styles of fracture-controlled permeability enhancement in faults and shear zones. *Geofluids*, *10*(1–2), 217–233. https://doi.org/10.1111/j.1468-8123.2010.00281.x

Cox, S. F. (2016). Injection-driven swarm seismicity and permeability enhancement: Implications for the dynamics of hydrothermal ore systems in high fluid-flux, over pressured faulting regimes—An invited paper. *Economic Geology*, *111*(3), 559–587. https://doi.org/10.2113/econgeo.111.3.559

Dorbath, L., Cuenot, N., Genter, A., & Frogneux, M. (2009). Seismic response of the fractured and faulted granite of Soultz-sous-Forêts (France) to 5 km deep massive water injections. *Geophysical Journal International*, *177*(2), 653–675. https://doi.org/10.1111/j.1365-246X.2009.04030.x

Evans, K. F., Moriya, H., Niitsuma, H., Jones, R. H., Phillips, W. S., Genter, A., et al. (2005). Microseismicity and permeability enhancement of hydrogeologic structures during massive fluid injections into granite at 3 km depth at the Soultz HDR site. *Geophysical Journal International*, *160*(1), 389–412. https://doi.org/10.1111/j.1365-246X.2004.02474.x

Fasola, S. L., Brudzinski, M. R., Holtkamp, S. G., Graham, S. E., & Cabral-Cano, E. (2019). Earthquake swarms and slow slip on a sliver fault in the Mexican subduction zone. *Proceedings of the National Academy of Sciences of the United States of America*, *116*(15), 7198–7206. https://doi.org/10.1073/pnas.1814205116

Fuhrman, M. L., & Lindsley, D. H. (1988). Ternary-feldspar modeling and thermometry. *American Mineralogist*, *73*, 201–215.

Galvez, M. E., Manning, C. E., Connolly, J. A. D., & Rumble, D. (2015). The solubility of rocks in metamorphic fluids: A model for rock-dominated conditions to upper mantle pressure and temperature. *Earth and Planetary Science Letters*, *430*, 486–498. https://doi.org/10.1016/j.epsl.2015.06.019

Ganzhorn, A. C., Pilorgé, H., & Reynard, B. (2019). Porosity of metamorphic rocks and fluid migration within subduction interfaces. *Earth and Planetary Science Letters*, *522*, 107–117. https://doi.org/10.1016/j.epsl.2019.06.030

Hack, A. C., & Thompson, A. B. (2011). Density and viscosity of hydrous magmas and related fluids and their role in subduction zone processes. *Journal of Petrology*, *52*(7–8), 1333–1362. https://doi.org/10.1093/petrology/egq048

Higashino, F., Rubatto, D., Kawakami, T., Bouvier, A., & Baumgartner, L. P. (2019). Oxygen isotope speedometry in granulite facies garnet recording fluid/melt–rock interaction (Sør Rondane Mountains, East Antarctica). *Journal of Metamorphic Geology*, *37*(7), 1037–1048. https://doi.org/10.1111/jmg.12490

Holland, T., & Powell, R. (1996). Thermodynamics of order-disorder in minerals: I. Symmetric formalism applied to minerals of fixed composition. *American Mineralogist*, *81*(11–12), 1413–1424. https://doi.org/10.2138/am-1996-11-1214

Holland, T. J. B., & Powell, R. (1998). An internally consistent thermodynamic data set for phases of petrological interest. *Journal of Metamorphic Geology*, *16*(3), 309–343. https://doi.org/10.1111/j.1525-1314.1998.00140.x

Holtkamp, S. G., & Brudzinski, M. R. (2011). Earthquake swarms in circum-Pacific subduction zones. *Earth and Planetary Science Letters*, *305*(1–2), 215–225. https://doi.org/10.1016/j.epsl.2011.03.004

Horálek, J., Jechumtálová, Z., Dorbath, L., & Šílený, J. (2010). Source mechanisms of micro-earthquakes induced in a fluid injection experiment at the HDR site Soultz-sous-Forêts (Alsace) in 2003 and their temporal and spatial variations. *Geophysical Journal International*, *181*(3), 1547–1565. https://doi.org/10.1111/j.1365-246X.2010.04506.x

Huber, M. L., Perkins, R. A., Laesecke, A., Friend, D. G., Sengers, J. V., Assael, M. J., et al. (2009). New international formulation for the viscosity of H_2O. *Journal of Physical and Chemical Reference Data*, *38*(2), 101–125. https://doi.org/10.1163/_q3_SIM_00374

Ide, S., Beroza, G. C., Shelly, D. R., & Uchide, T. (2007). A scaling law for slow earthquakes. *Nature*, *447*(7140), 76–79. https://doi.org/10.1038/nature05780

Ji, S., Shao, T., Michibayashi, K., Long, C., Wang, Q., Kondo, Y., et al. (2013). A new calibration of seismic velocities, anisotropy, fabrics, and elastic moduli of amphibole-rich rocks. *Journal of Geophysical Research E: Planets*, *118*(9), 4699–4728. https://doi.org/10.1002/jgrb.50352

John, T., Gussone, N., Podladchikov, Y. Y., Bebout, G. E., Dohmen, R., Halama, R., et al. (2012). Volcanic arcs fed by rapid pulsed fluid flow through subducting slabs. *Nature Geoscience*, *5*(7), 489–492. https://doi.org/10.1038/ngeo1482

Kanamori, H. (1977). The energy release in great earthquake. *Journal of Geophysical Research*, *82*(20), 2981–2987. https://doi.org/10.1029/jb082i020p02981

Kanamori, H., & Brodsky, E. E. (2004). The physics of earthquakes. *Reports on Progress in Physics*, *67*(8), 1429–1496. https://doi.org/10.1088/0034-4885/67/8/R03

Kao, H., Shan, S. J., Dragert, H., Rogers, G., Cassidy, J. F., Wang, K., et al. (2006). Spatial-temporal patterns of seismic tremors in northern Cascadia. *Journal of Geophysical Research*, *111*(3), 1–17. https://doi.org/10.1029/2005JB003727

Katayama, I., Terada, T., Okazaki, K., & Tanikawa, W. (2012). Episodic tremor and slow slip potentially linked to permeability contrasts at the Moho. *Nature Geoscience*, *5*(10), 731–734. https://doi.org/10.1038/ngeo1559

Kawakami, T., Higashino, F., Skrzypek, E., Satish-Kumar, M., Grantham, G., Tsuchiya, N., et al. (2017). Prograde infiltration of Cl-rich fluid into the granulitic continental crust from a collision zone in East Antarctica (Perlebandet, Sør Rondane Mountains). *Lithos*, *274–275*, 73–92. https://doi.org/10.1016/j.lithos.2016.12.028

Kleine, B. I., Zhao, Z., & Skelton, A. D. L. (2016). Rapid fluid flow along fractures at greenschist facies conditions on Syros, Greece. *American Journal of Science*, *316*(2), 169–201. https://doi.org/10.2475/02.2016.03

Kusebauch, C., John, T., Barnes, J. D., Klügel, A., & Austrheim, H. O. (2015). Halogen element and stable chlorine isotope fractionation caused by fluid-rock interaction (Bamble Sector, SE Norway). *Journal of Petrology*, *56*(2), 299–324. https://doi.org/10.1093/petrology/egv001

Kusebauch, C., John, T., Whitehouse, M. J., & Engvik, A. K. (2015). Apatite as probe for the halogen composition of metamorphic fluids (Bamble Sector, SE Norway). *Contributions to Mineralogy and Petrology*, *170*(4), 1–20. https://doi.org/10.1007/s00410-015-1188-6

Kusebauch, C., John, T., Whitehouse, M. J., Klemme, S., & Putnis, A. (2015). Distribution of halogens between fluid and apatite during fluid-mediated replacement processes. *Geochimica et Cosmochimica Acta*, *170*, 225–246. https://doi.org/10.1016/j.gca.2015.08.023

Lanari, P., Vidal, O., De Andrade, V., Dubacq, B., Lewin, E., Grosch, E. G., & Schwartz, S. (2014). XMapTools: A MATLAB©-based program for electron microprobe X-ray image processing and geothermobarometry. *Computers & Geosciences*, *62*, 227–240. https://doi.org/10.1016/j.cageo.2013.08.010

Liu, E. (2005). Effects of fracture aperture and roughness on hydraulic and mechanical properties of rocks: Implication of seismic characterization of fractured reservoirs. *Journal of Geophysics and Engineering*, *2*(1), 38–47. https://doi.org/10.1088/1742-2132/2/1/006

McGarr, A. (1976). Seismic moments and volume changes. *Journal of Geophysical Research*, *81*(8), 1487–1494. https://doi.org/10.1029/jb081i008p01487

McGarr, A. (2014). Maximum magnitude earthquakes induced by fluid injection. *Journal of Geophysical Research: Solid Earth*, *119*(2), 3678–3699. https://doi.org/10.1002/2013JB010597

Michel, S., Gualandi, A., & Avouac, J. P. (2019). Similar scaling laws for earthquakes and Cascadia slow-slip events. *Nature*, *574*(7779), 522–526. https://doi.org/10.1038/s41586-019-1673-6

Mindaleva, D., Uno, M., Higashino, F., Nagaya, T., Okamoto, A., & Tsuchiya, N. (2020). Rapid fluid infiltration and permeability enhancement during middle–lower crustal fracturing: Evidence from amphibolite–granulite-facies fluid–rock reaction zones, Sør Rondane Mountains, East Antarctica. *Lithos*, *372–373*, 105521. https://doi.org/10.1016/j.lithos.2020.105521

Mukuhira, Y., Asanuma, H., Niitsuma, H., Schanz, U., & Häring, M. (2008). Characterization of microseismic events with larger magnitude collected at Basel, Switzerland in 2006. In *Transactions: Geothermal Resources Council* (Vol. 32, pp. 87–94).

Mukuhira, Y., Uno, M., & Yoshida, K. (2022). Slab-derived fluid storage in the crust elucidated by earthquake swarm. *Communications Earth & Environment*, *3*, 286. https://doi.org/10.1038/s43247-022-00610-7

Nakajima, J., & Uchida, N. (2018). Repeated drainage from megathrusts during episodic slow slip. *Nature Geoscience*, *11*(5), 351–356. https://doi.org/10.1038/s41561-018-0090-z

Nakamoto, K., Hiramatsu, Y., Uchide, T., & Imanishi, K. (2021). Cascading rupture of patches of high seismic energy release controls the growth process of episodic tremor and slip events. *Earth Planets and Space*, *73*(1), 1–17. https://doi.org/10.1186/s40623-021-01384-6

Obara, K. (2002). Nonvolcanic deep tremor associated with subduction in southwest Japan. *Science*, *296*(5573), 1679–1681. https://doi.org/10.1126/science.1070378

Obara, K., & Hirose, H. (2006). Non-volcanic deep low-frequency tremors accompanying slow slips in the southwest Japan subduction zone. *Tectonophysics*, *417*(1–2), 33–51. https://doi.org/10.1016/j.tecto.2005.04.013

Oelkers, E. H., & Helgeson, H. C. (1988). Calculation of the thermodynamic and transport properties of aqueous species at high pressures and temperatures: Aqueous tracer diffusion coefficients of ions to 1000°C and 5 kb. *Geochimica et Cosmochimica Acta*, *52*(1), 63–85. https://doi.org/10.1016/0016-7037(88)90057-9

Ohmi, S., & Obara, K. (2002). Deep low-frequency earthquakes beneath the focal region of the M_w 6.7 2000 Western Tottori earthquake. *Geophysical Research Letters*, *29*(16), 54-1–54-4. https://doi.org/10.1029/2001gl014469

Osanai, Y., Nogi, Y., Baba, S., Nakano, N., Adachi, T., Hokada, T., et al. (2013). Geologic evolution of the Sør Rondane Mountains, East Antarctica: Collision tectonics proposed based on metamorphic processes and magnetic anomalies. *Precambrian Research*, *234*, 8–29. https://doi.org/10.1016/j.precamres.2013.05.017

Osanai, Y., Shiraishi, K., Takahashi, Y., Ishizuka, H., Tainosho, Y., Tsuchiya, N., et al. (1992). Geochemical characteristics of metamorphic rocks from Sør Rondane Mountains, East Antarctica.

Peacock, S. M. (2009). Thermal and metamorphic environment of subduction zone episodic tremor and slip. *Journal of Geophysical Research*, *114*(8), 1–9. https://doi.org/10.1029/2008JB005978

Peng, Z., & Gomberg, J. (2010). An integrated perspective of the continuum between earthquakes and slow-slip phenomena. *Nature Geoscience*, *3*(9), 599–607. https://doi.org/10.1038/ngeo940

Philpotts, A., & Ague, J. (2009). *Principles of igneous and metamorphic petrology*. Cambridge University Press.

Powell, R., & Holland, T. (1999). Relating formulations of the thermodynamics of mineral solid solutions: Activity modeling of pyroxenes, amphiboles, and micas. *American Mineralogist*, *84*(1–2), 1–14. https://doi.org/10.2138/am-1999-1-201

Rogers, G., & Dragert, H. (2003). Episodic tremor and slip on the Cascadia subduction zone: The chatter of silent slip. *Science*, *300*(5627), 1942–1943. https://doi.org/10.1126/science.1084783

Saito, S., Ishikawa, M., Arima, M., & Tatsumi, Y. (2016). Laboratory measurements of Vp and vs in a porosity-developed crustal rock: Experimental investigation into the effects of porosity at deep crustal pressures. *Tectonophysics*, *677–678*, 218–226. https://doi.org/10.1016/j.tecto.2016.03.044

Shelly, D. R. (2017). A 15 year catalog of more than 1 million low-frequency earthquakes: Tracking tremor and slip along the deep San Andreas Fault. *Journal of Geophysical Research: Solid Earth*, *122*(5), 3739–3753. https://doi.org/10.1002/2017JB014047

Shelly, D. R., Beroza, G. C., Ide, S., & Nakamula, S. (2006). Low-frequency earthquakes in Shikoku, Japan, and their relationship to episodic tremor and slip. *Nature*, *442*(7099), 188–191. https://doi.org/10.1038/nature04931

Shiraishi, K., Dunkley, D. J., Hokada, T., Fanning, C. M., Kagami, H., & Hamamoto, T. (2008). Geochronological constraints on the Late Proterozoic to Cambrian crustal evolution of eastern Dronning Maud Land, East Antarctica: A synthesis of SHRIMP U-Pb age and Nd model age data. *Geological Society, London, Special Publications*, *308*(1), 21–67. https://doi.org/10.1144/SP308.2

Sibson, R. H. (1994). Crustal stress, faulting and fluid flow. *Geological Society, London, Special Publications*, *78*(1), 69–84. https://doi.org/10.1144/GSL.SP.1994.078.01.07

Song, T. A., Helmberger, D. V., Brudzinski, M. R., Clayton, R. W., Davis, P., Pérez-campos, X., & Singh, S. K. (2009). Earthquakes in southern Mexico. *Science*, *502*(April), 502–507. https://doi.org/10.1126/science.1167595

Sweet, J. R., Creager, K. C., & Houston, H. (2014). A family of repeating low-frequency earthquakes at the downdip edge of tremor and slip. *Geochemistry, Geophysics, Geosystems*, *15*(9), 3713–3721. https://doi.org/10.1002/2014GC005449

Taetz, S., John, T., Bröcker, M., Spandler, C., & Stracke, A. (2018). Fast intraslab fluid-flow events linked to pulses of high pore fluid pressure at the subducted plate interface. *Earth and Planetary Science Letters*, *482*, 33–43. https://doi.org/10.1016/j.epsl.2017.10.044

Tan, Y. J., & Marsan, D. (2020). Connecting a broad spectrum of transient slip on the San Andreas fault. *Science Advances*, *6*(33), 1–9. https://doi.org/10.1126/sciadv.abb2489

Ujiie, K., Saishu, H., Fagereng, Å., Nishiyama, N., Otsubo, M., Masuyama, H., & Kagi, H. (2018). An explanation of episodic tremor and slow slip constrained by crack-seal veins and viscous shear in subduction mélange. *Geophysical Research Letters*, *45*(11), 5371–5379. https://doi.org/10.1029/2018GL078374

Uno, M., Okamoto, A., & Tsuchiya, N. (2017). Excess water generation during reaction-inducing intrusion of granitic melts into ultramafic rocks at crustal P–T conditions in the Sør Rondane Mountains of East Antarctica. *Lithos*, *284–285*, 625–641. https://doi.org/10.1016/j.lithos.2017.04.016

Vitovtova, V. M., Shmonov, V. M., & Zharikov, A. V. (2014). The porosity trend and pore sizes of the rocks in the continental crust of the Earth: Evidence from experimental data on permeability. *Izvestiya: Physics of the Solid Earth*, *50*(5), 593–602. https://doi.org/10.1134/S1069351314040181

Warren-Smith, E., Fry, B., Wallace, L., Chon, E., Henrys, S., Sheehan, A., et al. (2019). Episodic stress and fluid pressure cycling in subducting oceanic crust during slow slip. *Nature Geoscience*, *12*(6), 475–481. https://doi.org/10.1038/s41561-019-0367-x

Wech, A. G., Boese, C. M., Stern, T. A., & Townend, J. (2012). Tectonic tremor and deep slow slip on the Alpine Fault. *Geophysical Research Letters*, *39*(March), 1–6. https://doi.org/10.1029/2012GL051751

Wei, C., & Powell, R. (2003). Phase relations in high-pressure metapelites in the system KFMASH. *Contributions to Mineralogy and Petrology*, *145*(3), 301–315. https://doi.org/10.1007/s00410-003-0454-1

Zack, T., & John, T. (2007). An evaluation of reactive fluid flow and trace element mobility in subducting slabs. *Chemical Geology*, *239*(3–4), 199–216. https://doi.org/10.1016/j.chemgeo.2006.10.020